Available online at www.sciencedirect.com
SCIENCE DIRECT®
International Journal of Heat and Fluid Flow 25 (2004) 824–832
International Journal of HEAT AND FLUID FLOW
www.elsevier.com/locate/ijhff

Experimental and numerical investigation of turbulent natural convection in a large air-filled cavity

J. Salat [a], S. Xin [b], P. Joubert [c,*], A. Sergent [b], F. Penot [a], P. Le Quéré [b]

[a] LET-ENSMA, UMR CNRS 6608, BP 40109, 86961 Futuroscope Cedex, France
[b] LIMSI, UPR CNRS 3251, BP 133, 91403 Orsay, France
[c] LEPTAB, Université de La Rochelle, Avenue M. Crépeau, 17042 La Rochelle Cedex 1, France

Received 9 January 2004; accepted 21 April 2004
Available online 6 July 2004

Abstract

We investigate experimentally and numerically the turbulent natural convection flow that develops in a differentially heated cavity of height $H = 1$ m, width $W = H$ and depth $D = 0.32H$, submitted to a temperature difference between the active vertical walls equal to 15 K resulting in a characteristic Rayleigh number equal to 1.5×10^9. In the experiment temperature is measured by 25 μm micro-thermocouples and velocity by a Laser Doppler Anemometer. Both 2D and 3D LES and 3D DNS are performed. DNS uses a Chebyshev spectral method and LES a finite volume method with a local subgrid diffusivity model. Numerical simulations are performed for both adiabatic conditions and experimentally measured temperature on the horizontal walls. Time-averaged quantities and turbulent statistics in the median vertical plane are presented and compared.

Keywords: Turbulent natural convection; Differentially heated cavity; Experimental investigation; DNS and LES approaches

1. Introduction

Natural convection in cavities enjoys half-century long-lasting attention from the Computational Fluid Dynamics (CFD) and thermal science communities. For flow regime at high Rayleigh number, large-scale computations such as direct numerical simulation (DNS) and large eddy simulation (LES) are now becoming increasingly feasible and experimental measurements are more accurate and finer than in the past decades. However some basic questions still remain unanswered.

Stratification in the cavity core, for example, is still not well predicted: experimental studies yield a dimensionless stratification of about 0.5 while numerical simulations predict a value close to or even larger than 1. On the one hand, for width/height aspect ratios between 5 and 0.5, Cheesewright et al. (1986) reported an experimental value of 0.51, Mergui and Penot (1997) a value of 0.37 and Tian and Karayiannis (2000) a value of 0.50. On the other hand, 2D DNS and LES such as those performed by Le Quéré (1992), Xin and Le Quéré (1995), Nobile (2002) and Sergent et al. (2003) all reported a dimensionless stratification of about 1. Note that among 2D DNS those of Paolucci (1990) remains an exception in that the predicted stratification is equal to 0.38, but it turned out that the corresponding time integration was too short to reach the real asymptotic flow regime. 2D DNS and LES are thus not really successful as far as better agreement between experimental and numerical stratification is concerned, yielding the conclusion that some physical ingredients are lacking in the 2D Boussinesq equations with adiabatic top and bottom walls. The first step is to question the validity of the boundary conditions on the top and bottom walls, as actual measurements (1997) show temperature distributions far from those obtained assuming adiabaticity, and Le Quéré (1994) suggested that it was time to abandon adiabatic conditions for more realistic temperature distributions.

Another obvious limitation so far was the assumption of 2D flows, assumption imposed by the computing resources. The availability of increasing computing

* Corresponding author. Tel.: +33-54645-8624; fax: +33-54645-8241.
E-mail address: patrice.joubert@univ-lr.fr (P. Joubert).

0142-727X/$ - see front matter © 2004 Elsevier Inc. All rights reserved.
doi:10.1016/j.ijheatfluidflow.2004.04.003

Nomenclature

A_x, A_y	Aspect ratios of the cavity
D	cavity depth (m)
H	cavity height (m)
h_j	subgrid heat flux vector
$\overline{Nu}_0$, $\overline{Nu}_{MP}$	Nusselt number at the hot wall and along the median line
Pr	Prandtl number
Ra	Rayleigh number
$\overline{S}_{ij}$	resolved strain-rate tensor
t	time (s)
T	temperature (K)
$\overline{T}_{ij}$	subgrid thermal tensor
u_i	velocity component ($m\,s^{-1}$)
U	horizontal dimensionless velocity
x_i	Cartesian coordinate (m)
W	vertical dimensionless velocity

Greeks

α	thermal diffusivity ($m^2\,s^{-1}$)
$\overline{\Delta}$	filter characteristic size
ν	kinematic viscosity ($m^2\,s^{-1}$)
Φ_c	heat flux at the cut-off
τ_{ij}	subgrid stress tensor
θ	dimensionless temperature

Subscripts

c	relative to the cold wall
h	relative to the hot wall
SGS	relative to subgrid quantities

Superscripts

$\overline{(\cdot)}$	filtered quantity
$'$	time fluctuation

resources makes 3D computations, if not yet routine, at least feasible in the corresponding Rayleigh number range. Recently Peng and Davidson (2001) performed 3D LES for the experimental case investigated by Tian and Karayiannis (2000) and reported a better agreement between the measured stratification and LES prediction. This seems to indicate that 3D simulations would be more successful in predicting the thermal stratification in the cavity core. The same authors also concluded that one should use the measured temperature distributions on the top and bottom walls in 3D simulations.

The present joint effort was primarily undertaken to see if 3D simulations and the use of measured temperature distributions on the top and bottom walls in 3D simulations could help improving numerical predictions of global quantities such as temperature stratification. To this aim the authors made joint efforts, numerically and experimentally. A new experiment consisting of a cubic air-filled differentially heated cavity of 1 cubic meter was designed and built. Although in the experimental setup the use of guard cavities makes possible the investigation of different cavity depths, in the present work the cubic cavity has been divided into three equal-depth cavities and the central cavity with depth/height ratio of 0.32 was studied. The Rayleigh number investigated is equal to 1.5×10^9. Numerically, two 3D codes, using either a Chebyshev pseudo-spectral method or a finite volume discretization, were developed to perform 3D DNS and LES corresponding to the experiments. The present work aims at providing high quality experimental and numerical data for the benchmark problem of a differentially heated cavity at high Rayleigh number and at understanding the physical phenomena responsible of the discrepancy observed on the central thermal stratification between measurements and numerical simulations.

The present paper is organized as follows: the physical problem and a brief description of the experimental setup are first presented, followed by the description of the numerical methods that were used. Experimental and numerical results are then compared and analyzed before giving final discussion and concluding remarks.

2. Physical problem

We are interested in a fluid-filled cavity of width W, depth D, and height H, with two opposite vertical walls maintained at fixed temperatures T_h and T_c, the other walls being insulated. Due to buoyancy, a fluid motion is induced in the cavity, depending on the cavity geometry, the working fluid and the temperature difference, ΔT ($\Delta T = T_h - T_c$). In terms of dimensional analysis, the representative parameters are the geometrical aspect ratios ($A_x = W/H$ and $A_y = D/H$), the Prandtl number $Pr = \nu/\alpha$ and the Rayleigh number $Ra = (g\beta\Delta T H^3)/(\nu\alpha)$.

In the present work the cavity is filled with air ($Pr = 0.71$) and its size is fixed to $H = 1$ m, with $A_x = 1$ and $A_y = 0.32$. Therefore, air flow in the cavity will depend only on the temperature difference, ΔT. Two methodological approaches have been adopted to investigate the air flow at high Rayleigh number in this cavity: experimental measurements on the one hand and 3D numerical simulations on the other hand.

3. Experimental setup

The experimental facility is an air-filled differentially heated cavity of 1 m × 1 m × 1 m. Two opposite vertical

walls, made of 10 mm polished aluminium plate, are maintained at constant temperatures, T_h and T_c. The top and bottom walls act as adiabatic walls and are inserted between active walls. They are made of 10 cm polyurethane foam and covered by a 0.7 mm thick aluminium foil in order to reduce radiative absorption. The cavity is split into three cavities of equal size (1 m × 1 m × 0.32 m) by transparent polycarbonate sheets of 1 mm thick (Lexan®), as illustrated in Fig. 1. Measurements are done in the central cavity, while the two guard cavities insure lateral adiabatic condition for the central cavity. In addition, an extra-insulation is provided by two double glass panels.

In order to stay within the Boussinesq approximation, temperature difference between the hot and cold walls, ΔT, is kept equal to 15 K around the ambient temperature ($T_h = 303$ K and $T_c = 288$ K). Constant temperatures on these active walls are checked by 8 calibrated T-thermocouples. On the top and bottom walls, the thermal conditions which are supposed to be adiabatic can be precisely known thanks to the resolution of an inverse problem by using measurements from 10 T-type thermocouples judiciously located in polyurethane foams. The Rayleigh number based on the cavity height is equal to 1.5×10^9. Temperature and velocity profiles in the median plane of the central cavity ($y = 0.5A_y$) are measured at various positions.

Temperature measurements are obtained by two 25 μm K-type calibrated thermocouples placed at the end of a cane crossing the ceiling. 4096 samples are taken at each location. The sampling rate is fixed at 10 Hz. A three-dimensional displacement device allows one to move the cane through the central cavity with a spatial accuracy of 0.01 mm.

Velocity measurements are performed with a 5W two-components argon Laser Doppler Anemometer in backscatter mode. The volume of measurement is 0.1 mm in diameter, and 1.4 mm in length. A front lens with a 600 mm focal length is used. The resolution for the velocity is 6×10^{-5} m s^{-1} with a bandwidth of 0.125 MHz. Seeding is achieved with oil smoke, which produces particles of about 2 μm in diameter. For each data point, the number of readings depends on the local strength of the flow. Typically, measurements are stopped when one of the two following conditions is satisfied: either 40000 validated readings or duration of data acquisition longer than 7 min.

A more complete description of the experiment set-up and results can be found in Salat and Penot (2003).

4. Governing equations and numerical methods

We suppose that air in the cavity is Newtonian and incompressible and that the buoyancy-induced air flow is governed by the unsteady 3D Navier–Stokes equations under Boussinesq assumption. No-slip condition is applied on the cavity walls.

Numerical approximations of such flows can be achieved either by solving directly the unsteady 3D N–S equations with enough grid points (DNS) or by filtering the equations in time and modelling the Reynolds stresses (RANS approaches) or filtering the equations in space and modelling the subgrid dynamic stresses and heat flux (LES approaches). DNS provides instantaneous structure of full flow scales, and accurate statistics can be obtained for mean flow and turbulent quantities. High computation cost and its feasibility at only moderately high Rayleigh number are, however, the main drawbacks of this approach. On the other hand, LES models the effects of subgrid scales on the resolved scales but requires coarser grids than DNS. Higher Rayleigh numbers can thus be studied using LES. In order to investigate 3D natural convection flow in cavity by both

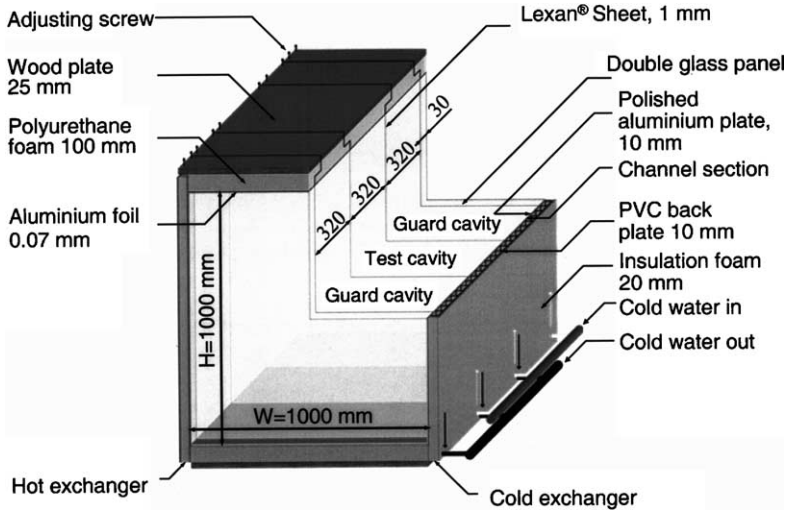

Fig. 1. Experimental setup.

DNS and LES, two 3D codes, one using a Chebyshev pseudo-spectral method and another using a finite volume description, were developed.

4.1. DNS via Chebyshev pseudo-spectral method

In the past, the authors performed 2D DNS by using Chebyshev pseudo-spectral method (Le Quéré, 1992; Xin and Le Quéré, 1995). Velocity-pressure coupling which is the main difficulty of solving the incompressible N–S equations has been tackled either by an influence matrix technique (Kleiser and Schumann, 1980) or by a direct Uzawa method (Bernardi and Maday, 1992). These methods assure that the velocity and pressure fields are coupled at the same time. Unfortunately, neither of these methods is feasible in 3D case, due to the huge dimensions of the influence matrix or Uzawa operator. An alternative method for 3D DNS is the projection method (Achdou and Guermond, 2000), but velocity and pressure fields are not evaluated exactly at the same time because of the time splitting. As DNS requires a high spatial resolution, and as a consequence small time steps, splitting error in time remains negligible. Velocity-pressure coupling is handled in two steps: in the first (prediction) step, the energy and momentum equations are solved by dropping the divergence-free condition but using the previous time step pressure; in the second (correction) step, the predicted velocity field is projected into divergence-free sub-space by solving a quasi-Poisson equation for the pressure correction. Details of the method can be found in (Xin and Le Quéré, 2002). The 3D pseudo-spectral code developed keeps most of the features of 2D one: the unsteady N–S equations are discretized in time by combining a BDF2 with a second-order Adams Bashforth extrapolation of convective terms; the resulting Helmholtz systems are solved by a direct solver based on full diagonalization of the discrete operators of second-order partial derivatives.

4.2. LES via finite volume method

For LES approach, a convolution filter is applied to the equations of motions and energy, and the resulting set of non-dimensional equations then reads:

$$\frac{\partial \bar{u}_i}{\partial x_i} = 0 \tag{1}$$

$$\frac{\partial \bar{u}_i}{\partial t} + \frac{\partial \bar{u}_i \bar{u}_j}{\partial x_j} = -\frac{\partial \bar{p}}{\partial x_i} + \frac{\partial}{\partial x_j}\left(Pr\, Ra^{-1/2}\left(\frac{\partial \bar{u}_i}{\partial x_j} + \frac{\partial \bar{u}_j}{\partial x_i} \right) \right) - \frac{\partial \tau_{ij}}{\partial x_j} + Pr\, \bar{\theta}\delta_{i1} \tag{2}$$

$$\frac{\partial \bar{\theta}}{\partial t} + \frac{\partial \bar{\theta}\bar{u}_j}{\partial x_j} = \frac{\partial}{\partial x_j}\left(Ra^{-1/2} \frac{\partial \bar{\theta}}{\partial x_j} \right) - \frac{\partial h_j}{\partial x_j} \tag{3}$$

These equations are made dimensionless by using the height of the cavity, H, as reference length, $[T - (T_h + T_c)/2]/(T_h - T_c)$ as reduced temperature and the natural convection characteristic velocity, $U_{CN} = \frac{\alpha}{H} Ra^{1/2}$. The Rayleigh number is defined as $Ra = \beta g \Delta T H^3/\nu\alpha$, and the Prandtl number as $Pr = \nu/\alpha$, where β is the volumetric thermal expansion coefficient, g is the acceleration due to the gravity, and ν and α are the molecular viscosity and diffusivity respectively.

The effects of the subgrid scales removed by the filtering operation on the resolved quantities ($\bar{\cdot}$) is accounted for by the subgrid-scale (SGS)stress tensors:

$$\tau_{ij} = \overline{u_i u_j} - \bar{u}_i \bar{u}_j \tag{4}$$

$$h_j = \overline{\theta u_j} - \bar{\theta}\bar{u}_j \tag{5}$$

The SGS stresses need to be modelled in terms of the resolved variables in order to close the equations. Most subgrid models are based on the definition of an eddy viscosity model and relate the deviatoric part of the subgrid tensor τ^d and the resolved strain-rate tensor $\bar{S}$, $\tau^d_{ij} = -2\nu_{SGS}\bar{S}_{ij}$, where ν_{SGS} is the subgrid viscosity and $\bar{S}_{ij} = \frac{1}{2}\left(\frac{\partial \bar{u}_i}{\partial x_j} + \frac{\partial \bar{u}_j}{\partial x_i}\right)$. In the same way, the SGS heat flux h_j is related to the large scale temperature gradient by a SGS diffusivity, α_{SGS}, as $h_j = -\alpha_{SGS}\frac{\partial \bar{\theta}}{\partial x_j}$. Usually, α_{SGS} is computed from ν_{SGS} assuming a Reynolds analogy $\alpha_{SGS} = \nu_{SGS}/Pr_{SGS}$ with the introduction of a subgrid Prandtl number which is severely approximated to be a constant. This amounts to considering that the small thermal scales depend solely on the resolved dynamic scales. Therefore it is suspected not to hold in the case of turbulent natural convection, where the flow is produced by buoyant forces and not through a dynamic forcing. We have thus developed a local subgrid diffusivity model (Sergent et al., 2003), along the lines of the Mixed Scale Viscosity Model (Sagaut, 1996). In this Mixed Scale Diffusivity Model, the subgrid diffusivity is expressed as the average of two models. The first one uses the thermal resolved scales, following the Smagorinsky approach (Smagorinsky, 1963), while the second is based on the subgrid scales (Turbulent Kinetic Energy approach, Bardina et al., 1980). The local diffusivity is then defined by:

$$\alpha_{SGS} = 0.5\frac{\bar{\Delta}^2}{\Delta\theta}|\overline{T}|^{1/2}|\phi_c|^{1/2} \tag{6}$$

where $|\overline{T}| = \sqrt{2\overline{T}_{ij}\overline{T}_{ij}}$ and $\overline{T}_{ij} = \frac{\partial \bar{\theta}}{\partial x_j}\overline{S}_{ij}$ (no summation on i and j). ϕ_c is the heat flux at the cut-off, which can be estimated following Bardina's similarity hypothesis (Bardina et al., 1980), by filtering the resolved velocity and temperature fields with a test filter coarser than the implicit one. The subgrid-scale dependency of this model ensures that it will adapt itself to the local state of the flow, and vanish in fully resolved regions of the flow and near the walls. Lastly, this thermal subgrid

diffusivity model allows to evaluate the subgrid diffusivity independently of the viscosity, and has been successfully applied to 2D natural convection in a differentially heated square cavity (Sergent et al., 2003). It is used in the present LES approach to assess its effectiveness in 3D cases.

An important point for LES of such flow is the near wall treatment. As in the Differentially Heated Cavity the flow is driven by the heat and momentum transfer at the wall, it is of primary importance to get an accurate description of the boundary layers. Two approaches can then be used: the first one is to use wall functions and the second is to directly solve the near-wall dynamics with a sufficiently fine grid. Taking advantage of the fact that the MSDM model vanishes naturally at the wall and does not need any dumping function, we then chose to refine the mesh near the wall using a tangent-hyperbolic law for the grid distribution. Our first point at the wall is located at $x^+ \approx 1$, and there is nearly 6 points in the thermal boundary layer, as recommended for example by Verzicco and Camussi (2003) for direct numerical simulation of turbulent thermal convection. Therefore no additional modelling other than the SGS model is introduced in the computations, which reduces the number of assumptions.

From a computational point of view, the 3D LES Finite Volume code is based on the same time scheme and projection method for velocity-pressure coupling as the DNS code. The spatial discretization is achieved on staggered grids. All the terms involved in the balance equations are evaluated with second-order accurate centered schemes, but a QUICK scheme is used for the nonlinear terms of the momentum equations. We have shown in Sergent et al. (2003) using an a priori test that the artificial dissipation induced by the QUICK approximation was able to well reproduce the energy transfer between resolved and unresolved scales of the flow. Therefore, we chose not to introduce a subgrid viscosity in the momentum equations, but only the above presented SGS-diffusivity model in the energy equation. The resulting Helmholtz equations are solved by an incremental ADI technique and the Poisson equation for pressure correction is solved by partial diagonalization of the discrete operators of spatial derivatives.

5. Results and discussions

All the following results are in dimensionless form.

5.1. Code validation and computational cases

Before considering the conditions of the experimental setup, the 3D codes were tested in the case of a cubic cavity under laminar conditions by comparison with the 3D spectral results of Tric et al. (2000). Table 1 summarizes the results of the comparison at $Ra = 10^7$, which is the higher Rayleigh number reported by these authors. A good agreement is observed for both finite volume and Chebyshev pseudo-spectral codes.

With regard to the experimental setup, we focused our effort on the $Ra = 1.5 \times 10^9$ regime, considering only few intermediate Rayleigh numbers without investigating transitions to time-dependent and chaotic flows. As adiabatic condition cannot be exactly prescribed in experiments, two cases were numerically considered for the top and bottom walls: one with adiabatic condition, and another with the experimental temperatures profiles. Table 2 reports the different simulations that were performed with their corresponding parameters. These simulations were performed on a NEC-SX5 supercomputer with running performances after optimization of respectively 2.5 GFlops for LES and 6.5 GFlops for DNS.

5.2. Time-averaged fields

In order to compare experimental and numerical 3D results to 2D results, the results are displayed in the median vertical plane ($y = 0.5A_y$).

Fig. 2 displays the measured temperature on the top and bottom walls and the corresponding profiles obtained with adiabatic conditions in numerical simulations. The experimental profiles were obtained from direct measurements very close to the cavity walls and confirmed by the results of an inverse heat conduction problem in the polyurethane foams, equipped with thermo-couples. On the one hand, imposing adiabatic horizontal walls yields the same wall temperature distribution for 2D LES and 3D DNS. On the other hand, numerical predictions of the wall temperature profiles

Table 1
Comparison with reference results (Tric et al., 2000) for a cubic cavity at $Ra = 10^7$

	Spatial resolution	$\overline{Nu_0}$	$\overline{Nu}_{MP}$	W_{max}
Tric et al. (2000)	$81 \times 81 \times 81$	16.342	16.547	0.2424
Finite volume code	$64 \times 32 \times 128$	16.338	16.544	0.2429
Chebyshev spectral code	$80 \times 80 \times 80$	16.342	16.547	0.2406

$\overline{Nu_0}$ denotes the mean Nusselt number at the hot wall, $\overline{Nu}_{MP}$ the averaged Nusselt number along the hot wall median line and W_{max} the maximum vertical velocity.

Table 2
Simulations performed at $Ra = 1.5 \times 10^9$ for the experimental setup and relevant parameters

	Horizontal walls	Spatial resolution	Time step	Integration time	Average time
2D LES	Adiabatic	64×128	0.005	500	450
3D LES	Experimental	$64\times32\times128$	0.008	600	400
3D DNS 1	Adiabatic	$150\times80\times180$	0.004	655	280
3D DNS 2	Experimental	$180\times100\times200$	0.002	266	234

Time step, integration time and average time are in dimensionless units of $Ra^{-1/2}H^2/\alpha$. Integration time represents the total integration time of unsteady N–S equations from a previous solution at lower Rayleigh number, and average time is the total time for computing turbulent statistics.

are very different from measurements and confirm the fact that the horizontal walls are not perfectly adiabatic. This is not surprising because air is a very poor heat conductor and it is extremely difficult to get a perfect insulation when using air as the working fluid. One can then expect that a better agreement between experimental and numerical studies could be achieved by using experimental data in numerical simulations, as done by Peng and Davidson (2001).

Fig. 3 (top) presents comparisons of experimental measurements of temperature and vertical velocity at mid-height of the cavity against numerical results.A good agreement is observed between experimental and numerical data. Note however that there is a small discrepancy between experiments and numerical simulations at $x \approx 0.02$: numerical simulations predict smaller values than experiments. The temperature profile is insensitive to the thermal boundary conditions on the top and bottom walls and to the type of numerical simulations (2D or 3D, DNS or LES). Vertical velocity does not depend on, as temperature, the type of numerical simulations but does react to the thermal boundary conditions on the top and bottom wall, and a better agreement is observed when considering the experimental temperature profiles.

Fig. 4 (top) display time-averaged results at mid-width of the cavity. For both temperature and horizontal velocity, the experimental results differ very much from the numerical predictions obtained by using adiabatic conditions on the horizontal walls. The use of experimental temperature profiles improves the numerical predictions for the horizontal velocity but for temperature, although discrepancy is reduced, differences still remain important. More, the thermal stratification at mid-height ($z = 0.5$) remains unchanged when considering the two types of boundary conditions.

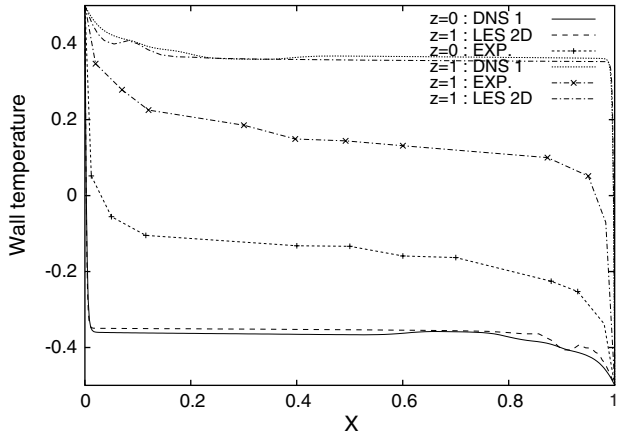

Fig. 2. Temperature distribution on the cavity horizontal walls.

5.3. Turbulent statistics

Temperature and velocity auto-correlations were measured and Figs. 3 and 4 (bottom) present measured turbulent statistics as well as DNS and 3D LES results. Note that due to the fact that temperature was measured by thermocouples and velocity by LDA, turbulent heat flux could not be obtained.

At mid-height of the cavity (Fig. 3), imposing adiabatic conditions (case DNS 1) results in a completely laminar flow as turbulent statistics in this case are too small to be seen on the figure. Using experimental profiles as thermal boundary conditions results in a more turbulent flow but numerical simulations then overestimate turbulent quantities.

At mid-width of the cavity, (Fig. 4), adiabatic horizontal walls result in small turbulent intensities while larger turbulent intensities are observed when using experimental profiles, especially for temperature. For the horizontal velocity variance (Fig. 4(d)), different shapes are observed between experimental and numerical values. While the experimental profile is quite regular, with only one maxima, the numerical results predict a wavy profile with two maxima, the first one located very near the horizontal wall, indicating probably Rayleigh-Bénard like turbulence, and the second one in the outer region of the horizontal boundary layer.

5.4. Heat transfer at the walls

Values of the averaged Nusselt number along the line $y = 0.5A_y$ of the hot wall are reported in Table 3 for the different cases considered. Once again, the 2D LES and 3D DNS values are in a fairly good agreement for the adiabatic horizontal walls. For the temperature imposed horizontal walls, the heat exchanges at the vertical walls are reduced compared to the adiabatic case. In this case LES and DNS slightly overestimate the heat transfer.

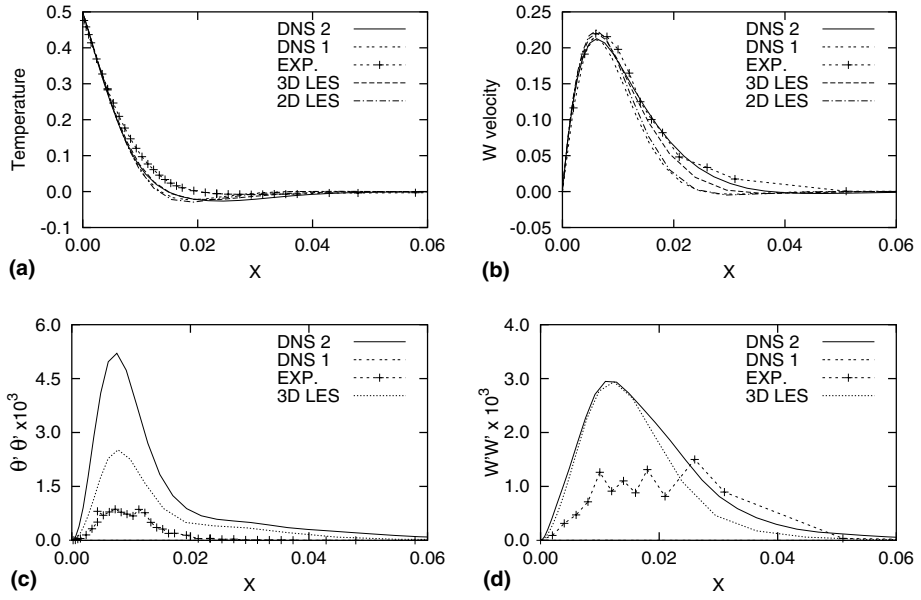

Fig. 3. Profiles at cavity mid-height in the median plan.

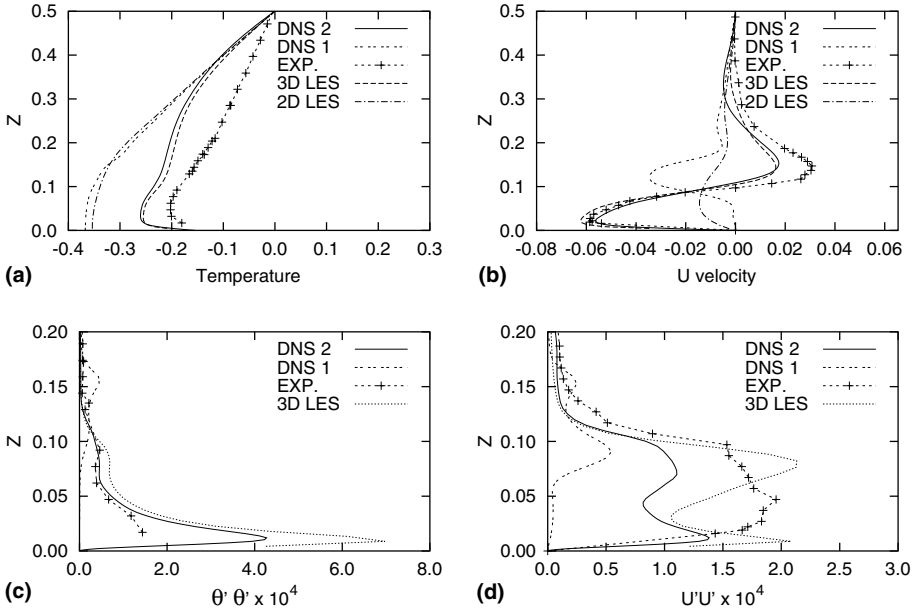

Fig. 4. Profiles at cavity mid-width in the median plan.

5.5. 3D versus 2D results

One goal in this study was to get an explanation for the observed differences between experimental results and our previous 2D DNS or LES results. An immediate possible reason for theses differences was of course to invoke 3D effects which cannot be taken into account by 2D computations. In fact, we observe here minor differences between 2D and 3D computations. The general features of the flow do not change dramatically, as long as only the mean values are concerned, and thus the origin of the discrepancies cannot be satisfactorily attributed to the 2D assumption. This is due to the fact that, as already observed by Dol and Hanjalić (2001), and Trias et al. (2003), the 3D effects are mainly encountered in the vicinity of the corners, while the general circulation in the cavity is mainly laminar and 2D. This conclusion reinforces a-posteriori the validity of previous 2D DNS or LES studies, but also allows one to use 2D approaches as a first and cheap attempt for investigating the general flow structure in cavities at Rayleigh numbers about 10^{10}.

Table 3
Comparaison of the averaged Nusselt number along the hot wall median line, $\overline{Nu}_{MP}$, for adiabatic or temperature imposed conditions on the horizontal walls

Adiabatic walls		Experimental distribution		
2D LES	DNS 1	3D LES	DNS 2	Exp.
61	60.1	57.5	58	54

6. Concluding remarks

A differentially heated cavity has been investigated experimentally and numerically. Our aim is to provide high quality experimental and numerical results in order to understand the discrepancy observed on the vertical thermal stratification in the core. To this aim, a new experiment was set up and two 3D codes were developed. Temperature and velocity fields have been measured in the experiment and various numerical simulations have been done.

When considering adiabatic horizontal walls, both 2D and 3D and both DNS and LES numerical simulations are consistent in the vertical median section. At cavity mid-height, there is a good agreement between experimental measurements and numerical simulations for the mean temperature and the vertical velocity. At cavity mid-width, as previously observed, the numerical results considerably differ from experimental measurements, especially in terms of the centerline thermal stratification and temperature distribution on the horizontal walls. This leads us to the conclusion that 2D numerical simulation is not the critical ingredient for explaining the discrepancy observed between numerical simulations and experiments for the thermal stratification.

Using experimentally measured temperature distributions along the top and bottom walls as boundary conditions in numerical simulations improves the agreement between experimental and numerical studies. We observe in this case a better agreement for the velocity field and velocity auto-correlations. Nevertheless, discrepancies on the centerline thermal stratification and temperature auto-correlation still remain important. We conclude that introducing experimental temperature measurements in numerical simulations is not the definitive answer to the discrepancy observed on the thermal stratification in the cavity core.

By a way of conclusion, despite the important efforts that were made, a discrepancy on the thermal stratification is still observed and it is concluded that some physical ingredients are still missing in order to understand the origin of this difference. We are presently developing a numerical model for the thermal boundary conditions on the lateral walls, which results from a subtle heat balance involving heat conduction in the polyurethane foams and aluminium foils as well as radiative transfer between the cavity walls. On the experimental side, measurements will be performed in order to check the adiabaticity hypothesis on the lateral walls of the test cavity.

Acknowledgements

Numerical simulations were performed on a NEC-SX5 supercomputer at IDRIS. Experimental set-up was supported by the French Ministry of National Education and Research within the AMETH program.

References

Achdou, Y., Guermond, J., 2000. Convergence analysis of a finite element projection/Lagrange–Galerkin method for the incompressible Navier–Stokes equations. SIAM J. Numer. Anal. 37, 799–826.

Bardina, J., Ferziger, J., Reynolds, W., 1980. Improved subgrid scales models for large eddy simulation. AIAA Paper 80–1357.

Bernardi, C., Maday, Y., 1992. Approximations spectrales de problèmes aux limites elliptiques. Springer Verlag.

Cheesewright, R., King, K., Ziai, S., 1986. Experimental data for the validation of computer codes for the prediction of two-dimensional buoyant cavity flows. In: Notes on Numerical Flow Dynamics, Vol. 60 of ASME Winter Annual Meeting, pp.75–81.

Dol, H.S., Hanjalić, K., 2001. Computational study of turbulent natural convection in a side-heated near-cubic enclosure at a high Rayleigh number. Int. J. Heat Mass Transfer 44, 2323–2344.

Kleiser, L., Schumann, U., 1980. Treatment of incompressibility and boundary conditions in three-dimensional numerical spectral simulations of plane channel flows, vol. 2 of Notes in Num. Fluid Mech. Vieweg, pp. 165–173.

Le Quéré, P., 1992. A modified Chebyshev collocation algorithm for direct simulation of 2D turbulent convection in differentially heated cavities. ICOSAHOM.

Le Quéré, P., 1994. Onset of unsteadiness, routes to chaos and simulations of chaotic flows in cavities heated from the side: a review of present status. In: Hewitt, G. (Ed.), Heat Transfer, vol. 1 of Proceedings of the 10th IHTC, pp. 281–296.

Mergui, S., Penot, F., 1997. Analyse des vitesse et température des l'air en convection naturelle dans une cavité carrée différentiellement chauffée à $Ra = 1.69 \times 10^9$. Int. J. Heat Mass Transfer 40, 3427–3441.

Nobile, E., 2002. Simulation of time-dependent flow in cavities with the additive-correction multigrid method, part II: applications. Numer. Heat Transfer Part B 30, 351–370.

Paolucci, S., 1990. Direct simulation of two dimensional turbulent natural transition in an enclosed cavity. J. Fluid Mech. 215, 229–262.

Peng, S., Davidson, L., 2001. Large eddy simulation for turbulent buoyant flow in a contained cavity. Int. J. Heat Mass Transfer 22, 323–331.

Sagaut, P., 1996. Numerical simulations of separated flows with subgrid models. Rech. Aérospatiale (English version) 1, 51–63.

Salat, J., Penot, F., 2003. Approche expérimentale de la convection naturelle en transition turbulente dans une cavité cubique différentiellement chauffée. VIe Colloque Interuniversitaire Franco-Québecois de Thermique des Systèmes, 26–28 mai 2003, Québec, pp. 75–81.

Sergent, A., Joubert, P., Le Quéré, P., 2003. Development of a local subgrid diffusivity model for large eddy simulation of buoyancy

driven flows: application to a square differentially heated cavity. Numer. Heat Transfer Part A 44 (8), 789–810.

Smagorinsky, J., 1963. General circulation experiments with the primitive equations i: the basic experiments. Month. Weath. Rev. 91 (3), 99–165.

Tian, Y., Karayiannis, T., 2000. Low turbulence natural convection in an air filled square cavity, part I and II. Int. J. Heat Mass Transfer 43, 849–884.

Trias, F.X., Soria, M., Pérez-Segarra, C.D., Oliva, A., 2003. DNS of natural convection in a differentially heated cavity: effects of the three-dimensional fluctuations. In: Proceedings of the International Symposium on Turbulence, Heat and Mass Transfer 4. Begell House Inc., pp. 409–416.

Tric, E., Labrosse, G., Betrouni, M., 2000. A first incursion into the 3d structure of natural convection of air in a differentially heated cubic cavity, from accurate numerical solutions. Int. J. Heat Mass Transfer 43, 4043–4056.

Verzicco, R., Camussi, R., 2003. Numerical experiments on strongly turbulent thermal convection in slender cylinder cell. J. Fluid Mech. 477, 19–49.

Xin, S., Le Quéré, P., 1995. Direct numerical simulations of two-dimensional chaotic natural convection in a differentially heated cavity of aspect ratio 4. J. Fluid Mech. 304, 87–118.

Xin, S., Le Quéré, P., 2002. An extended Chebyshev pseudo-spectral bench-mark for the 8:1 differentially heated cavity. Int. J. Num. Methods Fluids 40 (8), 981–998.